Surface Doping and Band Gap Tunability in Hydrogenated Graphene

ARTICLE *in* ACS NANO · DECEMBER 2011

Impact Factor: 12.88 · DOI: 10.1021/nn2034555 · Source: PubMed

6 AUTHORS, INCLUDING:

Felipe A Bulat
Pontifical Catholic University of Chile
30 PUBLICATIONS **1,190** CITATIONS
SEE PROFILE

Adam Friedman
United States Naval Research Laboratory
55 PUBLICATIONS **784** CITATIONS
SEE PROFILE

Surface Doping and Band Gap Tunability in Hydrogenated Graphene

Bernard R. Matis,[†] James S. Burgess,[†] Felipe A. Bulat,[‡] Adam L. Friedman,[§] Brian H. Houston,[⊥] and Jeffrey W. Baldwin[⊥,*]

[†]NRC Postdoctoral Associate, Naval Research Laboratory, Washington, D.C. 20375, United States, [‡]Sotera Defense Solutions Inc., Crofton, Maryland 21114, United States, [§]Naval Research Laboratory, Code 6361, Washington, D.C. 20375, United States, and [⊥]Naval Research Laboratory, Code 7130, Washington, D.C. 20375, United States

ABSTRACT

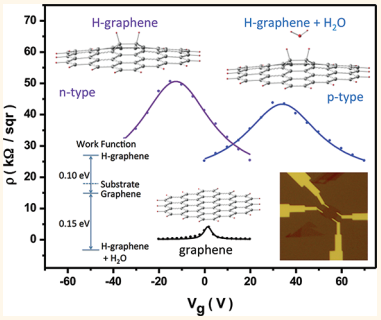

We report the first observation of the n-type nature of hydrogenated graphene on SiO_2 and demonstrate the conversion of the majority carrier type from electrons to holes using surface doping. Density functional calculations indicate that the carrier type reversal is directly related to the magnitude of the hydrogenated graphene's work function relative to the substrate, which decreases when adsorbates such as water are present. Additionally, we show by temperature-dependent electronic transport measurements that hydrogenating graphene induces a band gap and that in the moderate temperature regime [220−375 K], the band gap has a maximum value at the charge neutrality point, is tunable with an electric field effect, and is higher for higher hydrogen coverage. The ability to control the majority charge carrier in hydrogenated graphene, in addition to opening a band gap, suggests potential for chemically modified graphene p−n junctions.

KEYWORDS: graphene · hydrogenated graphene · transport · band gap · majority charge carrier

Graphene lacks a band gap in its electronic spectrum; thus graphene's conductivity cannot be turned off electronically as in conventional semiconductor materials.[1−3] The absence of a band gap is one of the biggest hurdles that must be overcome before graphene can be used as an electronic material for use in logic operations and one that has sparked an intense research effort to this effect. Chemical functionalization of graphene[4−6] is a promising method for tuning the material's unique band structure[7,8] and majority carrier type for future electronic and optical applications.[9−12]

Graphane, a recently discovered completely hydrogenated derivative of graphene,[4] is a stable two-dimensional structure in which the sp^2 C−C double bonds are hybridized to sp^3 C−C single bonds by the addition of hydrogen to the carbon lattice. Unlike graphene, which is a zero band gap semimetal, hydrogenated exfoliated and CVD-grown graphene has been shown to exhibit a strong temperature dependence ($\Delta R/\Delta T < 0$) characteristic of semiconducting materials.[4,13] Theoretically, the band gap of hydrogenated graphene has been shown to depend upon the amount of H coverage on each side of the graphene film as well as the distribution and ordering of H atoms on the film, reaching values as high as 5.4 eV.[9,14] Several recent experimental studies have shown that hydrogenated graphene has a band gap. Haberer *et al.* have used angle-resolved photoemission spectroscopy (ARPES) to measure a band gap in quasi-free-standing hydrogenated graphene on Au, where the size of the gap is tuned by varying the H/C ratio.[10] Additionally, Balog *et al.* using ARPES have shown that hydrogen adsorbed onto the Moire superlattice positions of graphene grown on an Ir(111) substrate also induces an appreciable band gap, which is tunable by varying the H/C ratio as well.[15] In spite of these significant achievements, many open questions still remain.

The extent to which the band gap can be tuned electrically has not been investigated, and little is known about the precise role of surface adsorbates on the majority carrier type. Here we show that hydrogenated graphene on SiO_2 is an n-type material and electrically demonstrate the ability to tune the band gap opening. We report on the ability to convert the majority carrier

* Address correspondence to jeffrey.baldwin@nrl.navy.mil.

Received for review September 7, 2011 and accepted December 21, 2011.

Published online December 21, 2011
10.1021/nn2034555

type from electrons to holes using surface adsorbates such as water, which according to our density-functional theory (DFT) model is a consequence of shifting of the material's work function relative to the substrate's work function upon hydrogenation and subsequent adsorption/desorption of atmospheric water. Furthermore, we demonstrate that in the temperature regime 220−375 K the band gap has a maximum value at the charge neutrality point (CNP), is tunable with an electric field effect, and is increases with the H/C ratio. This is the first report, to our knowledge, of the n-type nature of hydrogenated graphene on a SiO_2 substrate as well as the first demonstration of the complete reversibility of the majority carrier type with surface doping. The temperature-dependent resistivity of hydrogenated graphene shows semiconducting behavior and is well described by the variable-range hopping model. We show that in our devices a band gap of up to 50 meV emerges at the CNP and that the size of the gap can be tuned by varying V_g and/or the hydrogen coverage.

RESULTS AND DISCUSSION

Figure 1a is an optical micrograph of a typical graphene device (G-Sq) and electrical schematic used in our experiments. A Van der Pauw cross (referred to here as device X1) with arm dimensions of 500 and 200 nm (length and width, respectively) was characterized before (G-X1) and after hydrogenation (HG-X1). Figure 1b shows ρ *versus* V_g at 295 K for HG-X1+W (+W for "with adsorbed water") and illustrates both the increase in ρ and the shift in the CNP away from the pristine graphene state with increasing levels of hydrogenation, comparable to previously reported hydrogenated graphene studies.[4,16] The data shown in Figure 1b (with the exception of the purple trace) were intentionally taken as quickly as possible with each experiment commencing within 10 min of initiation of chamber evacuation ($P_o > 1.0 \times 10^{-4}$ Torr), thus not allowing for complete removal of physisorbed water. Ambipolar behavior is observed even for our highest D/G ratios, though ρ at the CNP is seen to increase by a factor of 11, and the CNP has shifted to the right nearly 30 V. The shift of the CNP to the right, indicating a larger fraction of p-type carriers, is attributed to atmospheric water adsorbed to the hydrogenated graphene surface. Such behavior indicates that the hydrogenated graphene is doped with holes, while water is adsorbed to the surface, and that the dopant level can be varied with different degrees of hydrogenation and/or surface water concentrations.

To remove the adsorbed water, the sample was heated while continuously maintaining a vacuum ($P < 1.0 \times 10^{-6}$ Torr). The purple trace in Figure 1b shows ρ *versus* V_g at 295 K after the device was heated to 375 K. Here, the CNP has shifted to negative V_g, a nearly 50 V shift, while ρ_{max} was seen to change by only

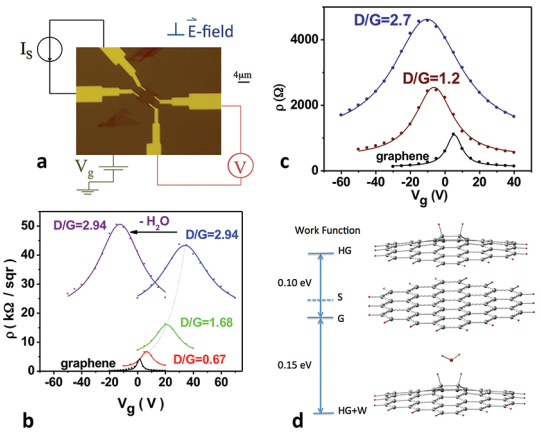

Figure 1. Shift of the CNP and maximum resistivity (ρ_{max}) with surface doping. (a) Optical image of a typical graphene device and electrical schematic. (b) ρ at 296 K as a function of V_g for graphene sample G-X1 (black trace) and three separate levels of hydrogenation (red, green, and blue traces) with water adsorbates (W). The solid curves are Lorentzian fits to the data. The dashed line is a guide to the eye. Purple trace: ρ *versus* V_g at 296 K for the D/G of 2.94 after heating to 375 K (HG-X1). The shift of the CNP to negative V_g demonstrates the conversion of the majority carrier type from p to n. (c) ρ *versus* V_g at 295 K for graphene sample G-Hb (black trace) and two separate levels of hydrogenation (red and blue curves) without water adsorbates. (d) Relative work functions of the graphene (G) (center), SiO_2 surface (S), hydrogenated graphene (HG) (top), and hydrogenated graphene with water adsorbates (HG+W) (bottom).

about 12% of its initial value. The shift of the CNP to negative V_g indicates that, without the presence of water on the surface, the hydrogenated graphene film has changed from p-type to n-type. Raman spectra collected after heating show that no measurable change occurs in the D/G ratio due to heating to 375 K, and we conclude that the change in hydrogen content after heating is negligible.

Figure 1c shows ρ *versus* V_g for device HG-Hb after having left the hydrogenated sample under vacuum for at least 24 h before any electrical measurements were carried out. Consistent with the slow removal of adsorbed water in a vacuum, the CNP is seen to shift to negative V_g values even without heating. The data in Figure 1c mirrors the symmetry seen about the graphene CNP in Figure 1b for hydrogenated graphene with adsorbed water and definitively shows that without water adsorbed to the film's surface, the hydrogenated graphene material is increasingly n-type for increasing levels of hydrogenation.

It is surprising that although the hydrogenated film displays n-type behavior, the incorporation of water—a known electron donor—physisorbed on the surface results in a p-type material. Our DFT model indicates that this behavior is due to changes in the materials work function (WF). While graphene's WF is very close to that of the substrate (thermal oxide on silicon), evidenced by its CNP being close to 0 V_g, the WF of the hydrogenated material is higher, leading to an electron enrichment of the film that accounts for our

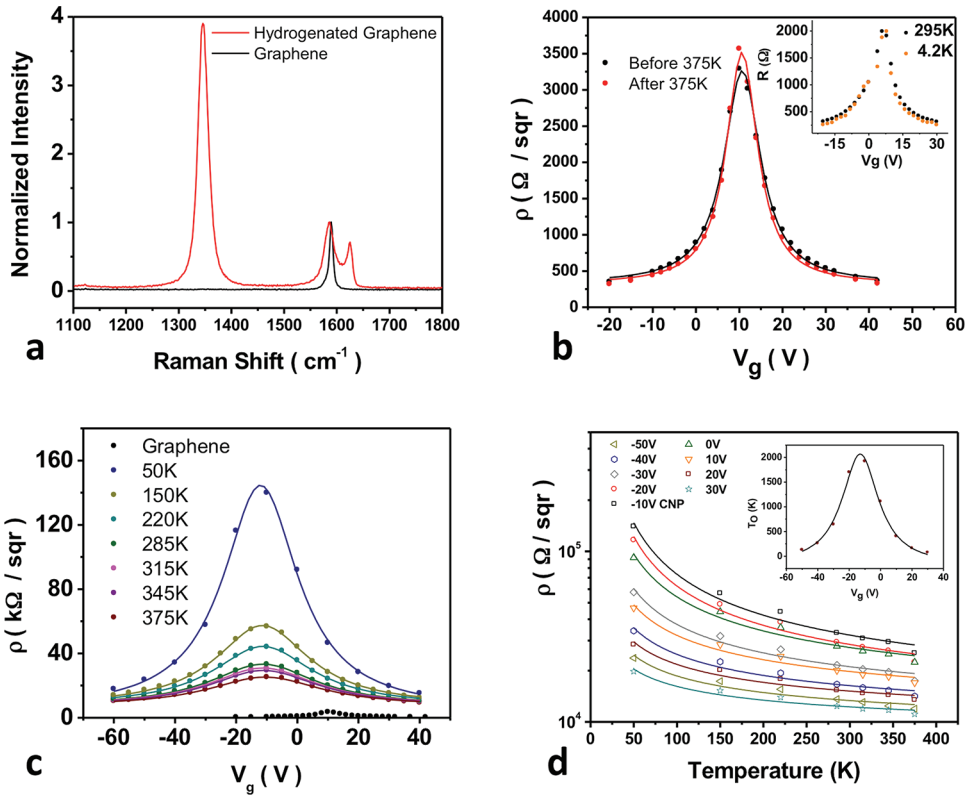

Figure 2. Electrical properties of n-doped hydrogenated graphene. (a) Raman spectra of the graphene device (square device) in (b)−(d) before (G-Sq) and after hydrogenation (HG-Sq). The spectra have been normalized to the G-mode intensity. (b) ρ as a function of V_g at 296 K for G-Sq before heating to 375 K (black trace) and after heating (red trace). The solid curves are Lorentzian fits to the data. Inset: temperature dependence of graphene demonstrates characteristic semimetallic properties. (c) ρ *versus* V_g from 50 to 375 K for the hydrogenated device HG-Sq with a D/G ratio of 3.9. Data were taken after pumping the chamber for 17 h. Note that the CNP is located at negative V_g, indicating an n-type material. The solid lines are Lorentzian fits to the data. The graphene (black trace) was measured at 295 K. (d) ρ *versus* T for several different gate voltages. The solid lines are fits to the VRH theory. Inset: Characteristic exponents T_o, extracted from a fit to the VRH theory, *versus* V_g. The black trace is a Lorentzian fit to the data.

observations (n-type). Furthermore, we observe that our model predicts that the physisorption of water leads to a significant lowering of the WF well below that of graphene (and thus that of the substrate), Figure 1d. A film WF lower than that of the substrate's results in an electron depletion (electrons moving from the film to the substrate), resulting in a p-type material. The different type of majority carriers is thus accounted for by the WFs of the different materials relative to the substrate, and such a striking change in majority carrier should be observed only in substrates whose WF is close to that of graphene.

The WF of graphene has been measured[17] and is almost identical to that of graphite, ~4.6 eV, very close to the reported value for a > 100 nm thermal oxide layer on n-type silicon,[18] which explains why our exfoliated graphene on a SiO_2 substrate always displays a CNP close to 0 V_g. As stated above, we performed DFT calculations to assess the effect of hydrogenation and subsequent water adsorption on the WF of graphene. For these purposes, we use a cluster model consisting of a coronene molecule using a triple-ζ Gaussian basis [6-311G(d,p)] and the wB97XD functional as implemented in the Gaussian 09 software suite.[19] To account for the effect of the positively charged substrate, we included an electric field in the direction perpendicular to the molecular plane. The relative changes on the WF were estimated by using the approximation WF = $-(e_{HOMO} + e_{LUMO})/2$. The WF for coronene is estimated to be 3.74 eV, and although this is about 0.9 eV lower than the experimental value for graphene, we are interested in its changes due to hydrogenation and subsequent water adsorption. The hydrogenated coronene displays a WF ~0.1 eV higher than that of coronene, while the absorption of water results in a lowering relative to coronene of ~0.15 to 0.20 eV, consistent with the discussion above. We emphasize the importance of accounting for the substrate effect through an electric field, as when no field is present, the WFs for the hydrogenated graphene material with and without water are both approximately ~0.06 eV lower than that of coronene.

We further study the electronic properties of the hydrogenated graphene with several additional devices including a square geometry (referred to here as device G-Sq) shown in Figure 1a and a cross geometry with arm dimensions of 1.25 μm by 500 nm (length and

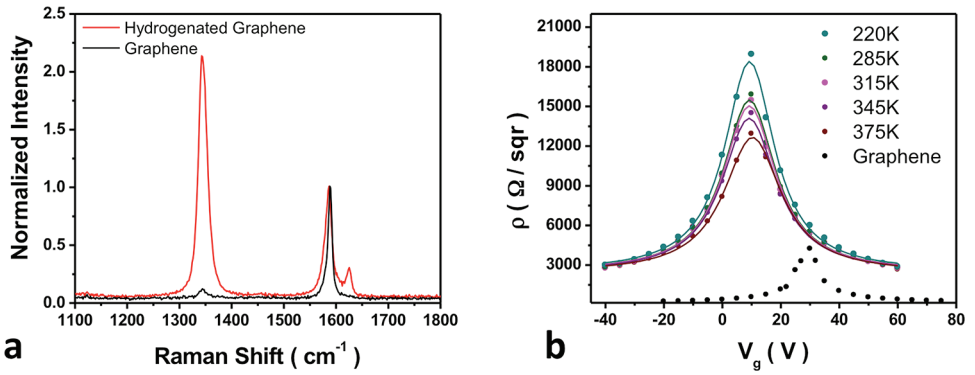

Figure 3. Electrical properties of p-type hydrogenated graphene before conversion to n-type. (a) Raman spectra of the graphene device (cross device) in (b) before (G-X2) and after hydrogenation (HG-X2). The spectra have been normalized to the G-mode intensity. (b) ρ *versus* V_g from 220 to 375 K for the hydrogenated device HG-X2 with a D/G ratio of 2.1. Data were taken after pumping the chamber for 17 h. Note that the CNP is to the left of the pristine graphene CNP, but to the right of 0 V_g. It is possible that this is due to unintentional doping of the initial graphene (CNP located at ~30 V). The solid lines are Lorentzian fits to the data. The graphene (black trace) was measured at 295 K.

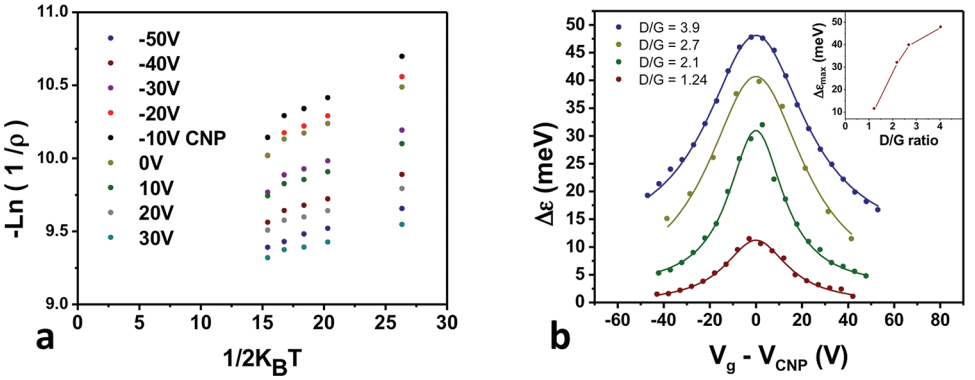

Figure 4. Band gap opening in hydrogenated graphene. (a) $-\ln(1/\rho)$ *versus* $1/2K_BT$ for the high-temperature data in Figure 2d. The band gap for a homogeneous semiconductor is the slope of the curve. (b) Band gap $\Delta\varepsilon$ *versus* $V_g - V_{CNP}$ for four different levels of hydrogenation. D/G ratio of 3.9: HG-Sq. D/G ratio of 2.1: HG-X2. D/G ratios of 1.24 and 2.7: HG-Hb. Solid curves are Lorentzian fits to the data. Inset: Maximum band gap *versus* D/G ratio, proves that a larger H/C ratio corresponds to a larger band gap at the CNP.

width, respectively, and referred to as device G-X2), which all demonstrate the same effect. The black traces in Figures 2c and 3b illustrate ρ *versus* V_g for the graphene found at 295 K. The graphene was heated to 375 K, and the CNP was determined to remain fixed in V_g at 295 K with no appreciable change in the ρ_{max} value, as seen in Figure 2b. The graphene 295 K mobility μ_h (p-type, hole conduction) for the G-Sq device was measured at 0 V_g and found to be 8300 $cm^2/(V\ s)$, while the 295 K temperature carrier density n_h was found to be $9.4 \times 10^{11}\ cm^{-2}$.

The two samples were hydrogenated to D/G ratios of 3.9 (HG-Sq) and 2.1 (HG-X2) and were evacuated in the cryostat for 17 h before any electrical measurements were carried out. The CNP for both hydrogenated samples shifted ~20 V to the left in V_g from the CNP of the pristine graphene even without heating, as can be seen in Figure 2c (HG-Sq) and Figure 3b (HG-X2). After the CNP had shifted the mobility and carrier density were measured for the HG-Sq sample at 0 V_g (n-type, $\mu_e = 307\ cm^2/V$, $n_e = 7.4 \times 10^{11}\ cm^{-2}$).

The samples were heated to 375 K though no appreciable change was observed in the location of the CNP. Thus we conclude that the majority of the water on the surface was desorbed during the extended time in vacuum. Together with the small changes in D/G ratios before and after the measurements and heating cycles, these observations indicate that the shift in carrier type is exclusively due to physisorption/desorption of water on the surface and not through a chemical reaction. Reversibility of the carrier type upon exposure of the film to atmospheric water further confirms this hypothesis, as the CNP was seen to shift back to the right after exposing the HG-Sq sample to deionized water and subsequently measuring ρ *versus* V_g.

We investigated ρ *versus* T in the 50 to 375 K range for the two different D/G ratios and at various V_g. Figures 2c and 3b show that ρ for each hydrogenated device changes sharply about the CNP with decreasing T, but that this change is not as severe when V_g is swept further away from the CNP. This semi-insulating behavior fits well to the two-dimensional variable range

hopping (VRH) theory described by eq 3, which is demonstrated in Figure 2d for the device with a D/G ratio of 3.9 (HG-Sq). The inset in Figure 2d plots the characteristic exponents T_o, found from the fit to the VRH theory, as a function of V_g, and is well fitted by a Lorentzian model. The values for ρ_o found from the VRH fit had a mean value of 5982 Ω/sqr and deviated from this value by no more than 20%.

$$\rho = \rho_o e^{\left(\frac{T_o}{T}\right)^{1/3}} \quad (3)$$

Changes in ρ as a function of T ($\Delta\rho/\Delta T$) increased with increasing levels of hydrogenation and suggest the opening of a band gap, $\Delta\varepsilon$. An estimate of $\Delta\varepsilon$ is deduced from the T dependence of the intrinsic conductivity σ ($1/\rho$), which for a homogeneous semiconductor varies exponentially, as shown in eq 4. Figure 4a plots the logarithmic behavior σ *versus* $1/2K_BT$, where the slope of the line should be proportional to the band gap.

$$\sigma \propto e^{-\Delta\varepsilon/2kT} \quad (4)$$

We find for each hydrogenated sample that the maximum band gap occurs at the CNP and decreases with V_g away from the CNP, as seen in Figure 4b. Furthermore, on the basis of the data in Figure 4b we conclude that a larger D/G ratio in the Raman spectra, and therefore a higher concentration of hydrogen atoms adsorbed to the graphene, will lead to a larger band gap opening at the CNP. Although a maximum $\Delta\varepsilon$ of ∼50 meV is measured in our lightly hydrogenated devices, we note that this is not a limit, as the calculated band gap for hydrogenated graphene increases up to 5.4 eV as you increase the hydrogen coverage.[9,14] We determine that the on/off ratio (the ratio of the low *vs* high resistance points in the R *vs* V_g plots) remains virtually fixed for graphene, but increases with decreasing temperature for hydrogenated graphene. For the data shown in Figure 2c the ratios of the two materials are approximately equivalent at 50 K, with the hydrogenated graphene on/off ratio increasing further with decreasing temperature. The fact that the on/off ratio for hydrogenated graphene is still low at room temperature could be the result of the creation of a small band gap (∼50 meV) and/or transport channels that are manifested within the band gap.

DFT calculations have been carried out within the plane-wave pseudopotential approximation[20,21] and indicate that for free-standing films (graphene, partially hydrogenated graphene, and partially hydrogenated graphene with water without accounting for substrate effects) there is a negligible band gap, which has been further confirmed by orbital-based DFT calculations that yield the same conclusion.[19] Also, the zero band gap in graphene has been shown to be very robust toward deformation and stress,[22−24] so that the stress induced by the substrate (which should be higher upon hydrogenation) does not account for the band gap either. We conclude that the observed band gap can be attributed to one or a combination of the following factors: (a) long-range disorder, (b) the large electric fields that a positively charged substrate such as thermal oxide would exert on the films, and (c) the electron density depletion/increase induced by the difference in WF between substrate and film.

The ability to control the majority carrier type while introducing a band gap makes hydrogenated graphene a promising method for nanocircuit design (*e.g.*, p−n junctions) in a graphene-based system. Tunability of the carrier type *via* surface doping removes the requirement for multiple gate electrodes for independent carrier type control, avoiding the need for high-quality dielectrics that are difficult to achieve on graphene and are susceptible to leakage currents. Our work also demonstrates how surface adsorbates can affect the electrical properties of hydrogenated graphene, properties that would otherwise be negligible in bulk materials.

EXPERIMENTAL METHODS

The graphene devices listed in Table 1 were fabricated by mechanical exfoliation of HOPG on a SiO_2 (275 nm)/Si (n-type arsenic doped) substrate,[25] followed by the deposition of Cr (10 nm)/Au (50 nm) contact electrodes. For devices that required additional geometrical patterning a low-power O_2 plasma treatment was used to etch the film into the desired shape. Hydrogenation of the graphene was performed according to ref 13 under the following conditions: 15−30 W, 1.5 Torr H_2, 100 sccm, 32 °C, for 15−30 s. The hydrogenation conditions (time and power) varied depending upon the desired level of hydrogenation. Raman spectroscopy was used to determine the relative defect densities in the films by a ratio of the G-mode intensity (1588 cm^{-1}, E_{2g} phonon mode) and the D-mode intensity (1345 cm^{-1}, appearing due to symmetry breaking at defect sites). The D/G ratio is related to the defect-free domain size of graphitic materials,[26,27] in this case caused by hydrogen addition to the graphene sheet. With the reactor conditions stated, the resulting D/G ratios demonstrated saturation for each power/time and were repeatable for all devices. Raman spectra were collected using a Renishaw MicroRaman spectrometer with a 514 nm laser excitation.

Electronic transport measurements were carried out in a cryogenic probe station, using ac lock-in techniques at a frequency of 13.7 Hz. A four-wire configuration is used in all of our measurements, as seen in Figure 1a. An excitation current of 10 nA was used for the hydrogenated devices (I = 31.6 nA for pristine graphene), and the voltage drop across the device was monitored and kept below K_BT/e to prevent charge carrier heating, where K_B is the Boltzmann constant and e the fundamental unit of electric charge. ρ for each device is found using eq 1, where I_{ab} is the source current along one edge of the sample and V_{cd} the voltage drop measured across the opposite edge (except for the Hall bar device G-Hb, in which case ρ is calculated from the resistance R *via* $\rho = RW/L$, where W and L are sample width and length, respectively).

$$\rho = \frac{\pi}{\ln 2}\frac{1}{4}\left(\frac{V_{43}}{I_{12}} + \frac{V_{14}}{I_{23}} + \frac{V_{21}}{I_{34}} + \frac{V_{32}}{I_{41}}\right) \quad (1)$$

TABLE 1. Properties of Graphene (G), Hydrogenated Graphene (HG), and Hydrogenated Graphene with Water Adsorbates (HG +W) for the Four Different Samples X1, Sq, X2, and Hb

sample	D/G ratio	CNP (V)	carrier type	ρ_{max} (at room T)
G-X1	0	1	p	4100 Ω/sqr
HG-X1+W	0.67	6	p	6800 Ω/sqr
	1.68	21	p	16 100 Ω/sqr
	2.94	34	p	43 300 Ω/sqr
	2.94	−13	n	51 000 Ω/sqr
HG-X1				
	0	10	p	3500 Ω/sqr
G-Sq	3.9	−11	n	33 300 Ω/sqr
HG-Sq				
	0	30	p	4200 Ω/sqr
G-X2	2.1	9	p	15 500 Ω/sqr
HG-X2				
G-Hb	0	6	p	1100 Ω
HG-Hb	1.24	−6.4	n	2500 Ω
	2.7	−10.3	n	4600 Ω

The Hall mobility of the charge carriers (μ) is calculated using eq 2, where the Hall resistance (R_H) and ρ were measured in a field of 220 mT. The values for the hydrogenated graphene were measured after the CNP had stopped shifting to the left in V_g, which under vacuum suggests that the majority of the water had been desorbed from the film's surface.

$$\mu = \frac{|R_H|}{\rho} \quad (2)$$

Acknowledgment. The authors gratefully acknowledge the members of the technical staff of the Institute for Nanoscience at NRL, David Zapotok and Dean St. Amand. The authors would also like to thank Daniel Gunlycke for useful discussions. B.R.M. and J.S.B. performed research courtesy of a National Research Council postdoctoral fellowship. This work was supported by the Office of Naval Research.

REFERENCES AND NOTES

1. Novoselov, K. S.; Geim, A. K.; Morozov, S. V.; Jiang, D.; Katsnelson, M. I.; Grigorieva, I. V.; Dubonos, S. V.; Firsov, A. Two-Dimensional Gas of Massless Dirac Fermions in Graphene. *Nature* **2005**, *438*, 197–200.
2. Geim, A. K.; Novoselov, K. S. The Rise of Graphene. *Nat. Mater.* **2007**, *6*, 183–191.
3. Tan, Y.-W.; Zhang, Y.; Bolotin, K.; Zhao, Y.; Adam, S.; Hwang, E. H.; Das Sarma, S.; Stormer, H. L.; Kim, P. Measurement of Scattering Rate and Minimum Conductivity in Graphene. *Phys. Rev. Lett.* **2007**, *99*, 246803.
4. Elias, D. C.; Nair, R. R.; Mohiuddin, T. M. G.; Morozov, S. V.; Blake, P.; Halsall, M. P.; Ferrari, A. C.; Boukhvalov, D. W.; Katsnelson, M. I.; Geim, A. K.; *et al.* Control of Graphene's Properties by Reversible Hydrogenation: Evidence for Graphane. *Science* **2009**, *323*, 610–613.
5. Robinson, J. T.; Burgess, J. S.; Junkermeier, C. E.; Badescu, S. C.; Reinecke, T. L.; Perkins, F. K.; Zalalutdinov, M. K.; Baldwin, J. W.; Culbertson, J. C.; Sheehan, P. E.; *et al.* Properties of Fluorinated Graphene Films. *Nano Lett.* **2010**, *10*, 3001–3005.
6. Englert, J. M.; Dotzer, C.; Yang, G.; Schmid, M.; Papp, C.; Gottfried, J. M.; Steinruck, H.-P.; Spiecker, E.; Hauke, F.; Hirsch, A. Covalent Bulk Functionalization of Graphene. *Nat. Chem.* **2011**, *3*, 279–286.
7. Novoselov, K. S.; Geim, A. K.; Morozov, S. V.; Jiang, D.; Zhang, Y.; Dubonos, S. V.; Grigorieva, I. V.; Firsov, A. A. Electric Field Effect in Atomically Thin Carbon Films. *Science* **2004**, *306*, 666–669.
8. Zhang, Y.; Tan, Y.-W.; Stormer, H. L.; Kim, P. Experimental Observation of the Quantum Hall Effect and Berry's Phase in Graphene. *Nature* **2005**, *438*, 201–204.
9. Gao, H.; Wang, L.; Zhao, J.; Ding, F.; Lu, J. Band Gap Tuning of Hydrogenated Graphene: H Coverage and Configuration Dependence. *J. Phys. Chem. C* **2011**, *115*, 3236–3242.
10. Haberer, D.; Vyalikh, D. V.; Taioli, S.; Dora, B.; Farjam, M.; Fink, J.; Marchenko, D.; Pichler, T.; Ziegler, K.; Simonucci, S.; *et al.* Tunable Band Gap in Hydrogenated Quasi-Free-Standing Graphene. *Nano Lett.* **2010**, *10*, 3360–3366.
11. Jeon, K.-J.; Lee, Z.; Pollak, E.; Moreschini, L.; Bostwick, A.; Park, C.-M.; Mendelsberg, R.; Radmilovic, V.; Kostecki, R.; Richardson, T. J.; *et al.* Fluorographene: A Wide Bandgap Semiconductor with Ultraviolet Luminescence. *ACS Nano* **2011**, *5*, 1042–1046.
12. Cheng, S.-H.; Zou, K.; Okino, F.; Gutierrez, H. R.; Gupta, A.; Shen, N.; Eklund, P. C.; Sofo, J. O.; Zhu, J. Reversible Fluorination of Graphene: Evidence of a Two-Dimensional Wide Bandgap Semiconductor. *Phys. Rev. B* **2010**, *81*, 205435.
13. Burgess, J. S.; Matis, B. R.; Robinson, J. T.; Bulat, F. A.; Perkins, F. K.; Houston, B. H.; Baldwin, J. W. Tuning the Electronic Properties of Graphene by Hydrogenation in a Plasma Enhanced Chemical Vapor Deposition Reactor. *Carbon* **2011**, *49*, 4420–4426.
14. Lebegue, S.; Klintenberg, M.; Eriksson, O.; Katsnelson, M. I. Accurate Electronic Band Gap of Pure and Functionalized Graphane from GW Calculations. *Phys. Rev. B* **2011**, *79*, 245117.
15. Balog, R.; Jorgensen, B.; Nilsson, L.; Andersen, M.; Rienks, E.; Bianchi, M.; Fanetti, M.; Laegsgaard, E.; Baraldi, A.; Lizzit, S.; *et al.* Bandgap Opening in Graphene Induced by Patterned Hydrogen Adsorption. *Nat. Mater.* **2010**, *9*, 315–319.
16. Jaiswal, M.; Haley, C.; Lim, Y. X.; Bao, Q.; Toh, C. T.; Loh, K. P.; Ozyilmaz, B. Controlled Hydrogenation of Graphene Sheets and Nanoribbons. *ACS Nano* **2011**, *5*, 888–896.
17. Yu, Y.-J.; Zhao, Y.; Ryu, S.; Brus, L. E.; Kim, K. S.; Kim, P. Tuning the Graphene Work Function by Electric Field Effect. *Nano Lett.* **2009**, *9*, 3430–3434.
18. Lindmayer, J. Heterojunction Properties of the Oxidised Semiconductor. *Solid-State Electron.* **1965**, *8*, 523–528.
19. Frisch, M. J.; Trucks, G. W.; Schlegel, H. B.; Scuseria, G. E.; Robb, M. A.; Cheeseman, J. R.; Scalmani, G.; Barone, V.; Mennucci, B.; Petersson, G. A.; *et al. Gaussian 09*, Revision A.1; Gaussian, Inc.: Wallingford, CT, 2009.
20. Giannozzi, P.; Baroni, S.; Bonini, N.; Calandra, M.; Car, R.; Cavazzoni, C.; Ceresoli, D.; Chiarotti, G. L.; Cococcioni, M.; Dabo, I.; *et al.* Quantum Espresso: a Modular and Open-Source Software Project for Quantum Simulations of Materials. *J. Phys.: Condens. Matter* **2009**, *21*, 395502.
21. Scandolo, S.; Giannozzi, P.; Cavazzoni, C.; Gironcoli, S.; de; Pasquarello, A.; Baroni, S. First-Principles Codes for Computational Crystallography in the Quantum−Espresso Package. *Zeit. Krist.* **2005**, *220*, 574.
22. Gui, G.; Li, J.; Zhong, J. Band Structure Engineering of Graphene by Strain: First-Principles Calculations. *Phys. Rev. B* **2008**, *78*, 075435.
23. Farjam, M.; Rafii-Tabar, H. Comment on "Band Structure Engineering of Graphene by Strain: First-Principles Calculations". *Phys. Rev. B* **2009**, *80*, 167401.
24. Gui, G.; Li, J.; Zhong, J. Reply to "Comment on `Band Structure Engineering of Graphene by Strain: First-Principles Calculations'". *Phys. Rev. B* **2009**, *80*, 167402.
25. Novoselov, K. S.; Jiang, D.; Schedin, F.; Booth, T. J.; Khotkevich, V. V.; Morozov, S. V.; Geim, A. K. Two-Dimensional Atomic Crystals. *Proc. Natl Acad. Sci. U. S. A.* **2005**, *102*, 10451–10453.
26. Tunistra, F.; Koenig, J. L. Raman Spectrum of Graphite. *J. Chem. Phys.* **1970**, *53*, 1126–1130.
27. Chen, J.-H.; Cullen, W. G.; Jang, C.; Fuhrer, M. S.; Williams, E. D. Defect Scattering in Graphene. *Phys. Rev. Lett.* **2009**, *102*, 236805.